

# Myopathy mutations in DNAJB6 slow conformer specific substrate processing that is corrected by NEF modulation

**Ankan Bhadra**

Washington University School of Medicine <https://orcid.org/0000-0002-8679-0984>

**Michael Rau**

Washington University in St. Louis <https://orcid.org/0000-0001-5170-2000>

**Jil Daw**

Washington University School of Medicine

**James Fitzpatrick**

Washington University in St. Louis <https://orcid.org/0000-0002-7907-3602>

**Conrad C. Wehl**

Washington University in St. Louis

**Heather True** (✉ [heather.true@WUSTL.EDU](mailto:heather.true@WUSTL.EDU))

Washington University School of Medicine <https://orcid.org/0000-0003-4824-9529>

---

## Article

### Keywords:

**Posted Date:** January 13th, 2022

**DOI:** <https://doi.org/10.21203/rs.3.rs-1041146/v1>

**License:** © ⓘ This work is licensed under a Creative Commons Attribution 4.0 International License.

[Read Full License](#)

---

**Version of Record:** A version of this preprint was published at Nature Communications on August 5th, 2022. See the published version at <https://doi.org/10.1038/s41467-022-32318-9>.

1 **Myopathy mutations in DNAJB6 slow conformer specific substrate**  
2 **processing that is corrected by NEF modulation**

3 Ankan K. Bhadra<sup>1</sup>, Michael J. Rau<sup>2</sup>, Jil A. Daw<sup>4</sup>, James A.J. Fitzpatrick<sup>1,2,3</sup>, Conrad C. Weihl<sup>4</sup>, Heather  
4 L. True<sup>1\*</sup>

5  
6 1. Department of Cell Biology and Physiology, Washington University School of Medicine, 660 South  
7 Euclid Avenue, Campus Box 8228, St. Louis, MO, 63110, USA. Electronic address:  
8 [heather.true@wustl.edu](mailto:heather.true@wustl.edu).

9 2. Washington University Center for Cellular Imaging (WUCCI), Washington University School of  
10 Medicine, St. Louis, United States.

11 3. Department of Neuroscience, Washington University School of Medicine, St. Louis, United States.

12 4. Department of Neurology, Hope Center for Neurological Diseases, Washington University School of  
13 Medicine, St. Louis, MO, USA.

14

15 **Abstract**

16 Molecular chaperones, or heat shock proteins (HSPs), protect against the toxic misfolding and  
17 aggregation of proteins. As such, mutations or deficiencies within the chaperone network can  
18 lead to disease. In fact, dominant mutations in DNAJB6 (Hsp40/Sis1), an Hsp70 co-chaperone,  
19 leads to a protein aggregate myopathy termed Limb-Girdle Muscular Dystrophy Type D1  
20 (LGMDD1). DNAJB6 client proteins and co-chaperone interactions in skeletal muscle are not  
21 known. Here, we used the yeast prion model client in conjunction with *in vitro* chaperone  
22 activity assays to gain mechanistic insights, and found that LGMDD1 mutants affect Hsp40  
23 functions. Strikingly, the mutants changed the structure of client protein aggregates, as  
24 determined by altered distribution of prion strains. They also impair the Hsp70 ATPase cycle,  
25 dimerization, and substrate processing and consequently poison the function of wild-type  
26 protein. These results define the mechanisms by which LGMDD1 mutations alter chaperone  
27 activity and provide avenues for therapeutic intervention.

28

29

## 30 **Introduction**

31 Limb-Girdle Muscular Dystrophies (LGMDs) are a genetically heterogeneous family of muscle  
32 disorders that are either as autosomal dominant or recessive<sup>1</sup>. Although most recessive LGMDs  
33 are characterized by a loss-of-function, the mechanistic nature of dominantly inherited LGMDs  
34 is unclear. These late onset degenerative myopathies are unified by similar myopathologies that  
35 include myofibrillar disorganization, impaired protein degradation, and the accumulation of  
36 protein inclusions that contain structural muscle proteins such as desmin and  $\alpha$ -actinin and RNA  
37 binding proteins such as TDP-43<sup>2-4</sup>. This toxic misfolding and aggregation of proteins is  
38 protected by the activity of molecular chaperones, or heat shock proteins (HSPs). As such,  
39 mutations in these chaperones can lead to diseases termed “chaperonopathies”. One such  
40 example is Limb-Girdle Muscular Dystrophy Type D1 (LGMDD1), caused by mutations in  
41 DNAJB6 (Hsp40), an Hsp70 co-chaperone<sup>4</sup>. The originally identified LGMDD1 disease  
42 mutations are present within the 12 amino acid stretch of the glycine/phenylalanine (G/F) rich  
43 domain<sup>3-7</sup>. DNAJB6 is expressed ubiquitously and participates in protein folding and  
44 disaggregation<sup>8-11</sup>; however, its role in skeletal muscle protein homeostasis is unknown. In  
45 addition, DNAJB6 client proteins and DNAJB6 chaperone interactions in skeletal muscle are not  
46 known. Fortunately, DNAJB clients are well-characterized in yeast and thereby afford a model  
47 system to study the effect of disease-causing mutants. Moreover, the understanding of DNAJB  
48 function within the yeast chaperone network is more complete than in skeletal muscle.  
49 Previously, we utilized a transdisciplinary approach to ascertain the functionality of LGMDD1-  
50 associated mutants in model systems<sup>12</sup>. Here, we generated homologous DNAJB6 LGMDD1  
51 G/F domain mutations in the essential yeast DNAJ protein Sis1 (DNAJB6-F93L (Sis1-F106L),  
52 DNAJB6-N95L (Sis1-N108L), DNAJB6-D98 $\Delta$  (Sis1-D110 $\Delta$ ), and DNAJB6-F100I (Sis1-  
53 F115I)). Our goal is to accelerate our understanding of mutant DNAJB6 dysfunction in  
54 LGMDD1 and thus facilitate therapeutic target identification as well as to gain insight into the  
55 relationship between protein quality control and myopathy.

56 The Hsp70/DNAJ machinery is vital to the protein quality control network. The Hsp70  
57 machine works in an ATP-dependent manner to act on client proteins through a cycle of  
58 regulated binding and release<sup>13</sup>. Client specificity of the Hsp70 machine is modulated by DNAJ  
59 proteins (Hsp40s). By dictating client specificity, DNAJ proteins have been described as the

60 primary facilitators of the cellular protein quality control system and play a pivotal role in  
61 determining the fate of a misfolded protein – whether is refolded or degraded<sup>13</sup>. A variety of  
62 disease-associated misfolded proteins have been shown to interact or colocalize with DNAJ  
63 family members<sup>8,14</sup>. These effects are generally, although not exclusively, dependent upon  
64 cooperation with Hsp70<sup>8,13</sup>. Strikingly, previous work from our lab suggests that the LGMDD1  
65 mutants not only show substrate specificity, but also show conformation-specific  
66 effects<sup>12,15</sup>. These results were obtained through analysis of LGMDD1 mutants in the DNAJ  
67 protein Sis1, which has well-known yeast prion protein clients. Unlike mammalian prions, yeast  
68 prions are non-toxic, but phenotypic and biochemical assays developed enable rapid detection of  
69 [PRION+] cells<sup>16</sup>. Yeast chaperones Hsp104, Hsp70 (Ssa1), and the Hsp40 (Sis1) regulate prion  
70 propagation by acting on prion protein aggregates<sup>17</sup>. Alterations in chaperone level or function  
71 result in a failure to promote prion propagation<sup>18,19</sup>.

72 One of the most interesting features of prions is the existence of prion strains. Prion  
73 strains are distinct self-propagating protein aggregate structures that cause changes in  
74 transmissibility and disease pathology with the same aggregating protein<sup>20</sup>. Yeast prion strains  
75 differ from each other based on phenotype, the ratio of soluble to aggregated protein, and their  
76 ability to propagate the prion<sup>20</sup>. Previously, we found that homologous LGMDD1 mutations in  
77 Sis1 appear to reduce functionality, as determined by changes in their ability to modulate the  
78 aggregated state of select yeast prion strains<sup>12</sup>. We then assessed the effect of these mutants in  
79 mammalian systems, including mouse models, and LGMDD1 patient fibroblasts, where we  
80 analyzed the aggregation of TDP-43, an RNA binding protein with a prion-like domain that is a  
81 marker of degenerative disease including LGMDD1. DNAJB6 mutant expression enhanced the  
82 aggregation and impaired the dissolution of nuclear stress granules containing TDP-43 following  
83 heat shock<sup>12</sup>. Recently, three novel pathogenic mutations associated with aberrant chaperone  
84 function that leads to LGMDD1 have been identified within the J domain of DNAJB6<sup>21</sup>.  
85 Interestingly, we found that homologous mutations in the Sis1 J domain differentially alter the  
86 processing of specific yeast prion strains, as well as a non-prion substrate<sup>15</sup>.

87 Here, we used the yeast prion model system, and *in vitro* chaperone activity assays to  
88 determine how LGMDD1 homologous missense mutations in the Sis1 G/F domain alter  
89 chaperone function with and without Hsp70. We found that LGMDD1 mutants inhibit the  
90 Hsp70 ATPase cycle function in a client-conformer specific manner. Moreover, both prion

91 propagation and luciferase refolding activity were enhanced in mutant strains by either deleting  
92 the NEF (Sse1) or by using Sse1-mutants, indicating that fine-tuning of substrate processing can  
93 rescue the mutant defects. To our knowledge, this is the first mechanistic insight describing the  
94 effect of LGMDD1 mutants on Hsp70/40 ATPase cycle. Additionally, these results suggest that  
95 the development of a titrated approach using specific inhibitors of the Hsp70/DNAJ cycle is a  
96 potential therapeutic strategy for this class of myopathy-associated chaperonopathies.

97

## 98 **Results**

### 99 **1. LGMDD1-associated homologous G/F domain mutants in Sis1 have variable substrate** 100 **processing efficiency.**

101 In previous studies, we analyzed the functionality of LGMDD1 mutants in Sis1 using two yeast  
102 prion proteins that require Sis1 for propagation: Rnq1 (which forms the [RNQ+] prion) and  
103 Sup35 (which forms the [PSI+] prion). We found that LGMDD1 mutants had conformer-  
104 specific processing defects, in that they promoted the propagation of some prion strains but not  
105 all<sup>12</sup>. This suggests that the mutant chaperones may recognize their normal clients in some  
106 conformations but not others. Alternatively, the mutant chaperones may recognize clients but not  
107 be able to effectively process the misfolded protein. Hsp40 client processing for refolding  
108 requires multiple steps: binding, dimerization, binding to Hsp70, and nucleotide exchange-  
109 stimulated client release. We evaluated the function of LGMDD1 mutants as compared to wild  
110 type (WT), using assays that address these steps.

111 One way to determine substrate processing of a chaperone that interacts with  
112 amyloidogenic proteins is to evaluate the kinetics of aggregation of client proteins *in vitro*. We  
113 assessed amyloid formation of Rnq1 in the presence of Sis1-WT and LGMDD1 mutants (G/F  
114 domain mutants Sis1-F106L, Sis1-N108L, Sis1-D110Δ and, Sis1-F115I). Rnq1 is a well-known  
115 substrate of Sis1<sup>22</sup> and has been reported to form higher-order aggregates *in vitro*<sup>23</sup>. Aggregation  
116 of Rnq1 was monitored by the enhanced fluorescence emission of the dye Thioflavin T (ThT),  
117 which is used as a marker for cross β sheet conformation of amyloid fibrils<sup>24</sup>. During the initial  
118 phase of incubation (lag phase), natively disordered protein monomer did not show any change  
119 in fluorescence intensity of ThT (Fig. 1A). This was followed by an increase in ThT fluorescence  
120 intensity, indicative of the formation of fibrils. Finally, the fluorescence intensity of the dye

121 achieved a plateau (stationary phase). The lag phase was increased in the presence of Sis1-WT as  
122 compared to Rnq1 without chaperones (Fig. 1A), indicating that the time required for productive  
123 nucleation of unseeded Rnq1 was longer in the presence of chaperone. However, the lag phase of  
124 Rnq1 fiber formation was shorter with LGMDD1 mutants than Sis1-WT but longer than that of  
125 Rnq1 alone (Fig. 1A). The overall fibril formation rate was also higher in the presence of the  
126 mutants as compared to Sis1-WT (Fig. 1A). We also performed seeded kinetic assays with Rnq1  
127 fibers formed at 18°C, 25°C and 37°C. We found that fiber elongation was faster (in the absence  
128 of chaperone) with seeded Rnq1 at 18°C, than at 25°C or 37°C (Fig.S1A, B, and C). Similarly, in  
129 the presence of Sis1-WT, the difference in fiber elongation using Rnq1 seeds formed at the three  
130 temperatures was negligible (Fig.S1A, B, and C). This suggests that the primary impact of Sis1  
131 on Rnq1 fiber formation is in amyloid-competent conformer formation (nucleation) in the lag  
132 phase. Formation of aggregates was also assessed by semi-denaturing agarose gel electrophoresis  
133 (SDD-AGE). Rnq1 monomer showed a soluble band with no aggregates, while fibers of Rnq1  
134 showed higher molecular weight aggregates (Fig. S1D).

135 We then hypothesized that, if the primary chaperone effect is to alter the nucleation of the  
136 amyloidogenic protein, the fibers formed with and without chaperone could be structurally  
137 distinct. As such, we assessed the morphology of Rnq1 fibrils formed at 18°C with and without  
138 chaperone by Transmission Electron Microscopy (TEM). TEM images show that Rnq1 forms  
139 long, elongated, branched fibrils in the absence of chaperone (Fig. 1B). By contrast, Rnq1 fibers  
140 formed in the presence of Sis1-WT were short and appeared immature or perhaps bound to  
141 chaperone (Fig. 1B). This suggests that Sis1-WT might only delay fibril formation rather than  
142 preventing it. In the presence of LGMDD1 mutant (Sis1-F115I), very few fibers were visible  
143 (Fig. 1B) and they were mostly distorted and appeared to be small oligomeric species. These data  
144 suggest that the interaction of LGMDD1 mutants with client change the conformation of client in  
145 a manner that is distinct from that of wildtype chaperone.

146 While the interaction with prion substrate showed that LGMDD1 mutants alter amyloid  
147 formation, DNAJ proteins typically act in conjunction with Hsp70 to process substrates. We then  
148 asked whether the LGMDD1 mutants could promote substrate refolding in the presence of co-  
149 chaperones. Previously Aron et. al. showed that Sis1 lacking the domain that harbors these  
150 LGMDD1 mutants (Sis1 $\Delta$ G/F) is defective in chaperone activity and partially inhibits the ability

151 of Sis1-WT to facilitate folding of denatured luciferase protein<sup>25</sup>. Therefore, to test the ability of  
152 LGMDD1 mutants to function in substrate refolding, we heat-denatured firefly luciferase and  
153 then monitored refolding in the presence or absence of chaperones. We found that the LGMDD1  
154 mutants were all compromised in their ability to refold luciferase (Fig. 1C). Taken together,  
155 these results indicate that the LGMDD1 mutants are defective in substrate processing.

## 156 **2. LGMDD1-associated G/F domain mutants change the formation of *in vitro* formed** 157 **[RNQ+] prion strains.**

158 Given the striking differences in fibril formation kinetics and TEM images, we wanted to  
159 determine whether LGMDD1 mutants alter the formation of Rnq1 amyloid structures using a  
160 more sensitive and quantitative method that is uniquely available in the yeast prion system. This  
161 entails infecting yeast with amyloid generated *in vitro* and assessing the resulting [RNQ+] prion  
162 strains. Previously, we found that amyloid fibers of Rnq1PFD (prion-forming domain) formed at  
163 different temperatures resulted in the generation of different prion strains<sup>26</sup>.

164 We hypothesized that Rnq1 amyloid structure, and resulting [RNQ+] strain distribution, would  
165 differ in the presence of Sis1 and LGMDD1 mutants. We formed Rnq1 fibers at 18°C in the  
166 presence and absence of Sis1-WT and two LGMDD1 mutants. We transformed fibers formed in  
167 the presence or absence of chaperone into cells expressing [RNQ+] reporter protein (RRP) that  
168 did not have the prion ([*rnf-*]) (Fig. S2A). We developed and utilized this reporter strain as a  
169 phenotypic indicator of [RNQ+] prion strain propagation<sup>26</sup>. By assessing colony color (white,  
170 light pink, or dark pink) as well as growth on selective medium (SD-Ade), we scored [RNQ+]  
171 strains (Fig. 2A and B) that resulted after fiber infection. Lighter colony color and more growth  
172 on SD-Ade medium was scored as a stronger [RNQ+] strain, whereas darker colony color and  
173 less growth on selective medium was scored as a weaker [RNQ+] strain (see Methods for more  
174 information). [RNQ+] strains were also verified for the prion-specific trait of curability on  
175 medium containing guanidine hydrochloride (Fig. 2A and B). To quantify the difference in  
176 [RNQ+] strains formed in the presence of LGMDD1 mutants we counted the phenotype of  
177 infected colonies from five different transformation sets for each sample (Fig. 2C). With Rnq1  
178 alone, ~58% of cells showed very weak [RNQ+] phenotypes. This fraction of very weak [RNQ+]  
179 was reduced to less than 20% in the presence of Sis1-WT and was further reduced in the  
180 presence of the LGMDD1 mutants. There was a significant increase in the medium [RNQ+]

181 strain phenotype (44% +/- 4.5%) in the presence of Sis1-WT as compared to Rnq1 alone (14%  
182 +/- 1.4%). When we compared [RNQ+] strain distribution between Sis1-WT and LGMDD1  
183 mutants, we found that the proportion of weak Rnq1 strains was significantly increased with both  
184 F106L and F115I (~20% in Sis1-WT vs. 50% in F106L and 65% in F115I). Similarly, the  
185 population of medium [RNQ+] strain was significantly decreased in F115I as compared to Sis1-  
186 WT (~20% in F115I vs. 45% in Sis1-WT). The distribution of other [RNQ+] strains, strong and  
187 very weak, in LGMDD1 mutants were similar to Sis1-WT. Taken together, the difference in  
188 distribution of [RNQ+] strains in the presence of LGMDD1 mutants establish both the  
189 conformer-specific effects and suggest that the LGMDD1 mutants are not simply loss-of-  
190 function mutants as the [RNQ+] strains generated are markedly different than those arising in the  
191 absence of chaperone.

### 192 **3. LGMDD1-associated homologous mutants in Sis1 (Hsp40) alters its ability to function** 193 **with Ssa1 (Hsp70) efficiently.**

194 Hsp40s target substrates to their Hsp70 partners and regulate the ATPase activity and substrate  
195 binding of the Hsp70<sup>13</sup>. The recognition of substrates depends on their conformation, and it has  
196 been suggested that much of the Hsp40 conformation-dependent recognition is dependent on the  
197 G/F domain<sup>22,27-29</sup>. Thus, we evaluated the ability of LGMDD1 mutants to function in  
198 conjunction with Ssa1. We measured the ability of Sis1-WT and LGMDD1 mutants to stimulate  
199 the ATPase activity of Ssa1 in the presence and absence of different Rnq1 protein conformers.  
200 We standardized the Rnq1 monomer concentration and performed a phosphate standard curve  
201 with each assay (Fig. S3A). Notably, there was no difference in ATP hydrolysis rate between  
202 Sis1-WT and LGMDD1 mutants in the absence of any client protein (Fig. S3B). However, the  
203 ATP hydrolysis rate was significantly reduced with the mutants in the presence of Rnq1 seeds  
204 formed at 18°C and 25°C (Fig. 3A and B). Interestingly, the ATP hydrolysis rate of all mutants  
205 was marginally but not significantly reduced as compared to Sis1-WT in the presence of Rnq1  
206 seeds formed at 37°C (Fig. 3C). We found no difference in ATP hydrolysis rate between Sis1-  
207 WT and LGMDD1 mutants in the presence of Rnq1 monomer (denatured) as client (Fig. 3D).  
208 This may be due to the fact that “denatured monomer” presents a variety of epitopes that can be  
209 recognized by chaperone whereas the fibers likely have fewer sites for recognition. These results

210 indicate that the LGMDD1 mutants' ability to stimulate the ATPase activity of Ssa1 is  
211 conformer-dependent.

#### 212 **4. LGMDD1 G/F domain mutants alters both substrate and Hsp70 binding**

213 There are multiple facets that determine the efficiency of Hsp70-40 ATPase cycle. One of the  
214 key initial steps is the ability of Hsp40 to bind to client. Thus, we wanted to test the physical and  
215 functional interactions of LGMDD1 mutants with our Rnq1 and luciferase substrates. We  
216 performed a binding assay utilizing a method previously used to study interactions between the  
217 *E. coli* DnaJ and substrates<sup>30</sup>. We found that LGMDD1 mutants show significantly reduced  
218 binding to denatured Rnq1 and luciferase substrates as compared to Sis1-WT (Fig. 4A and B) at  
219 low concentrations of substrate. Once the mutants bind substrate, however, they are able to  
220 stimulate Hsp70 activity (Fig. 3D).

221 A key function for Hsp40s is stimulating Hsp70s. Based on our previous work, we hypothesized  
222 that the deleterious effect of the DNAJB6 G/F domain mutants is HSP70-dependent<sup>31</sup>. Thus, the  
223 LGMDD1 mutants might be altered in their productive association with Hsp70. These mutants  
224 may affect the cycle by either reducing Hsp70 binding, sequestering Hsp70, or they may be  
225 hyperactive and alter the refolding process. We found that reducing the interaction of LGMDD1  
226 mutants with Hsp70 using pharmacologic compounds led to improvement in muscle strength and  
227 myopathology in mouse models<sup>31</sup>. Therefore, we performed binding assays to determine whether  
228 there was a productive association between the LGMDD1 mutants and Ssa1. We found that the  
229 interaction between LGMDD1 mutants and Ssa1 was significantly reduced both in the absence  
230 (Fig. S4) and presence of client proteins Rnq1 (Fig. 4C) and luciferase (Fig. 4D). This indicates  
231 that the reduced interaction between the mutants and Ssa1 is client-independent.

#### 232 **5. LGMDD1 G/F domain mutants show reduced dimerization efficiency.**

233 The efficient function of Sis1 requires the ability of the protein to form dimers. In fact, Sis1 (1–  
234 337aa), which lacks the dimerization motif, exhibited severe defects in chaperone activity, but  
235 could regulate Hsp70 ATPase activity<sup>32</sup>. Sha et. al. proposed that the Sis1 cleft formed in dimers  
236 functions as a docking site for the Hsp70 peptide-binding domain and that this interaction  
237 facilitates the transfer of peptides from Sis1 to Hsp70<sup>33</sup>. Thus, in order to further evaluate the  
238 chaperone activity of the LGMDD1 mutants, we set out to measure their dimerization efficiency.

239 We performed binding assays to determine the relative competence of both the self-association  
240 of the mutants as well as their association with Sis1-WT. We found that there was a significant  
241 decrease in self-association of all the mutants as compared to Sis1-WT (Fig. 5A). We also found  
242 that their ability to bind to Sis1-WT was significantly reduced (Fig. 5B), indicating a possible  
243 explanation for the reduction in chaperone activity observed with these mutants.

## 244 **6. LGMDD1 G/F domain mutants inhibit Sis1-WT induced Ssa1 ATPase activity by** 245 **reducing its dimerization and substrate binding efficiency.**

246 Due to the dominant nature of these mutants, we set out to test the effect of LGMDD1 mutants  
247 on the Sis1-WT induced ATPase activity of Ssa1 in the presence of different client-conformers.  
248 For this, we performed an ATPase assay with mixtures of Sis1-WT and LGMDD1 mutants;  
249 F106L and F115I in the presence of Rnq1 fibers formed at two different temperatures, 18°C and  
250 25°C. We found that there was a gradual decrease in the rate of ATP hydrolysis that correlated  
251 with titrating Sis1-WT with F106L (Fig. 6A and S5A) and F115I (Fig. 6B and S5B).

252 Efficient ATP hydrolysis is a culmination of many small but significant events related to the  
253 individual function of Sis1 (Hsp40), Ssa1 (Hsp70) and other players in the ATP-hydrolysis  
254 cycle. Two critical aspects of Sis1-WT activity are its ability to dimerize and to bind to substrate  
255 efficiently. LGMDD1 mutants show decreased dimerization as compared to wild-type protein  
256 (Fig 5A and B). Thus, we decided to determine whether the mutants also inhibit the ability of  
257 wild-type protein to dimerize. We found that there was a concomitant decrease in dimerization  
258 with the titration of Sis1-WT with F106L (Fig. S6A) and F115I (Fig. S6B). We asked whether  
259 the mutants also inhibit the ability of wild-type protein to bind substrates efficiently. The binding  
260 efficiency to both substrates, Rnq1 (Fig. S6C) and luciferase (Fig. S6D), were slightly but  
261 significantly reduced when Sis1-WT was used in equal proportion (1:1) with each of the  
262 LGMDD1 mutants F106L and F115I. These data provide mechanistic insight into the inhibition  
263 of Sis1-WT-induced Ssa1 ATPase activity in the presence of LGMDD1 mutants (Fig. 6).

## 264 **7. Modulating Hsp40-Hsp70 cycle by either deleting or inhibiting nucleotide exchange** 265 **factors (NEFs) can be beneficial with respect to LGMDD1 G/F mutant effect *in vivo*.**

266 The lifetime of the Hsp70/40:substrate complex is dependent upon nucleotide exchange. A key  
267 player in this is nucleotide exchange factors (NEFs) that stimulate ADP release. In yeast,

268 cytosolic Hsp70 interacts with three NEFs homologous to human counterparts: Sse1/Sse2  
269 (Hsp110), Fes1 (HspBP1), and Sn11 (Bag-1)<sup>34,35</sup>. Previously, we found that LGMDD1 mutants  
270 impair viability and prion propagation in yeast and these effects were rescued by reducing the  
271 association with Hsp70<sup>31</sup>. Thus, we decided to investigate whether deleting Hsp110 (Sse1) would  
272 have a similar rescuing effect. A significant effect would further support the hypothesis that  
273 Hsp70 activity inhibition provides a potential mechanism for therapeutic intervention for  
274 LGMDD1-associated myopathy. To assess the impact of NEFs, we asked whether their deletion  
275 would enhance the ability of LGMDD1 mutants to propagate [RNQ+] prion strains. We used two  
276 established biochemical yeast prion assays that differentiate soluble and aggregated protein:  
277 well-trap and boiled gel assays. We found that the deletion of Sse1 partially rescues [RNQ+]  
278 prion propagation (Fig. 7A, S7A). However, it was specific to Sse1, as the alteration of the other  
279 NEFs did not demonstrate such rescuing (Fig. S7B). This was not surprising, as Sse1 is the  
280 principal NEF in yeast and performs 90% of the NEF activity in the cell<sup>36</sup>.

281 Based on these data, we hypothesized that fine-tuning the inhibition of Hsp70 activity could have  
282 a positive phenotypic effect with respect to LGMDD1 mutants. Thus, we assessed the effect of  
283 characterized Sse1 mutants that inhibit Hsp70 activity either by delaying binding to the Hsp70-  
284 client-ADP complex (Sse1-K69Q) or by delaying the release of ADP from the Hsp70-client  
285 complex (Sse1-G233D)<sup>37</sup>. We performed boiled gel assays to examine the relative levels of  
286 soluble Rnq1 prion protein in [RNQ+] cells. Indeed, we found a decrease in soluble Rnq1 protein  
287 (like in Sse1-WT cells expressing Sis1-WT) in LGMDD1 cells expressing either Sse1-G233D  
288 (Fig. S7C) or Sse1-K69Q (Fig. S7D). This indicates restoration of [RNQ+] prion propagation in  
289 LGMDD1 mutants with NEF modulation. This further supports our hypothesis that fine-tuning  
290 Hsp70 activity could provide a therapeutic avenue for LGMDD1.

291 To further understand the impact of Sse1 on the LGMDD1 disease-associated mutants, we  
292 assessed the refolding of a non-prion substrate (firefly luciferase; FFL). We utilized an *in vivo*  
293 refolding assay in which FFL is denatured in cells by heat shock and its subsequent refolding,  
294 which requires the Hsp40/Hsp70/Hsp104 chaperone machinery, is measured by activity<sup>38,39</sup>. We  
295 transformed the Sse1 and  $\Delta$ sse1 yeast cells carrying Sis1-WT, LGMDD1 mutants, and Sse1  
296 mutants with GPD-lux vector for the expression of FFL. Since Hsp104 is required for efficient  
297 refolding of FFL, we used a  $\Delta$ hsp104 strain expressing FFL as a negative control. We found that

298 the FFL refolding activity was significantly altered in Sse1 cells expressing F115I as compared  
299 to cells expressing Sis1-WT (Fig. 7B). This difference in FFL refolding activity between  
300 LGMDD1 mutants (F115I) and Sis1-WT was non-existent in *Δsse1* yeast cells (Fig. 7B).  
301 However, we observed that the FFL refolding activity was marginally higher in *Δsse1* yeast cells  
302 expressing F115I as compared to Sse1-WT cells expressing the same mutant protein (Fig. 7B).  
303 Interestingly, *Δsse1* yeast cells co-expressing F115I and Sse1 mutant (Sse1-G233D) showed  
304 significant improvement in FFL refolding activity as compared to Sse1-WT yeast cells (Fig. 7B).  
305 This improvement in FFL refolding activity with Sse1- mutants correlated with the improvement  
306 of Rnq1 prion propagation observed in *Δsse1* yeast cells (Fig. S7C and S7D). As cellular  
307 homeostasis depends upon the efficient functioning of the entire chaperone machinery, our  
308 results indicate that LGMDD1 mutants delay Hsp70 ATPase activity, possibly resulting in the  
309 increased load of aggregation-prone muscular proteins observed in LGMDD1 patients.

## 310 **Discussion**

311 Proper functioning of protein chaperones, including that of Hsp70/DNAJ, is important for the  
312 maintenance of muscle function<sup>40</sup> (Fig. 8A). Previously, we have shown that the LGMDD1  
313 mutations in the G/F domain of DNAJB6 disrupt client processing in both a substrate- and  
314 conformation-specific manner<sup>12</sup>. Here, we delved into the mechanism underlying the defect in  
315 client processing shown by LGMDD1 G/F domain mutants. Our data show that the LGMDD1  
316 mutants inhibit the Hsp70 ATPase activity (Fig. 8B), which may result in general impairment of  
317 protein quality control and accumulation of protein inclusions in muscle.  
318 Indeed, we demonstrated using the yeast prion model system which affords a unique  
319 conformer:phenotype read-out. Prion proteins can form several unique prion variants (or strains)  
320 that have slight differences in their  $\beta$ -sheet structure that constitute distinct amyloid  
321 conformations<sup>41</sup>. Such different structures are presumably the underlying cause of the diverse  
322 phenotypic variation seen in both yeast and prion diseases<sup>20</sup>. Several mammalian pathological  
323 proteins have also been shown to adopt distinct self-propagating aggregates or “strains” with  
324 different structures, which are presumably linked to the phenotype diversities of degenerative  
325 diseases<sup>16,42–44</sup>. One such example is Tau protein, deposition of whose pathological forms results  
326 into Tauopathies, which includes Alzheimer’s disease, Fronto-Temporal Dementia (FTD).  
327 Several studies support the “tau strain hypothesis”, which proposes that different aggregated tau

328 conformers (distinct strains) have distinct pathology-initiating capacities because they interact  
329 with endogenous tau differently<sup>45,46</sup>. In yeast, interaction between the prion protein Rnq1 and the  
330 Hsp40 Sis1 is required for [RNQ+] propagation<sup>29</sup>. Therefore, we utilized this system to ask  
331 whether the LGMDD1 mutants impacted the [RNQ+] prion strains that form *de novo*. Strikingly,  
332 we found a change in [RNQ+] prion strain formation when Rnq1 protein had formed fibers in the  
333 presence of the LGMDD1 mutants as compared to wild type Sis1. These changes were a direct  
334 consequence of Hsp40 interaction alone and may be a consequence of DNAJ proteins ability to  
335 act as “*holdases*”<sup>47,48</sup>. “*Holdases*” are chaperones that do not use ATP and simply protect their  
336 client protein from aggregation<sup>48</sup>. Unlike “*holdases*”, “*foldases*” (like Hsp70) accelerate the  
337 transition of non-native conformations towards native states in an ATP-dependent manner.  
338 Interestingly, the proteostasis network relies on a constant interplay between these two kinds of  
339 chaperones. Our results suggest that the “*holdase*” activity associated with LGMDD1 mutants is  
340 compromised and this alters substrate folding.

341 As a major role for Hsp40s is stimulating Hsp70s, another important aspect of the  
342 LGMDD1 mutants might be a change in the productive interaction with Hsp70<sup>25</sup>. Indeed, we  
343 found that these LGMDD1 mutants were defective in binding to Ssa1 (Hsp70) as well as to  
344 substrates (Rnq1 and luciferase). It had been shown previously that there was no difference in the  
345 ATPase activity between Sis1-WT and the Sis1-G/F domain knockout in absence of substrate<sup>25</sup>.  
346 However in our case, the introduction of the LGMDD1 mutants led to reduction in the ATPase  
347 activity of Hsp70. Moreover, in the presence of substrate, the change in ATPase activity was  
348 client-conformer specific, as assays with Rnq1 fibers formed at 18°C and 25°C showed reduced  
349 activity, while Rnq1 monomer did not. Additionally, LGMDD1 mutants were defective in  
350 refolding heat-denatured luciferase (similar to previous findings with Sis1ΔG/F<sup>25</sup>), indicating a  
351 more global defect in substrate remodeling. These findings correlate well with recent data that  
352 implicate the G/F-rich region of DNAJB1 in an autoinhibitory mechanism that regulates the  
353 major class B J-domain proteins (JDPs)<sup>49</sup>. Thus, although in all JDPs the interaction of the J-  
354 domain is responsible for the activation of Hsp70, in DNAJB1, due to this autoinhibitive  
355 interaction with the G/F domain, the activation of Hsp70 is inhibited. This inhibition can be  
356 released with second site mutations (E50A, or F102A, and or ΔH5) on DNAJB1<sup>49</sup>. As DNAJB6  
357 (Sis1) belongs to the same class B JDPs, a similar mechanism of interaction is likely, and  
358 mutations in the G/F domain could disrupt the autoinhibitory mechanism. Additionally, this is

359 consistent with recent observation, where we have found that aggregation-independent toxicity  
360 induced by the overexpression of the Sis1 LGMDD1 F106L and F115I mutants in yeast can be  
361 rescued by reducing Hsp70 binding<sup>31</sup>. These results confirm that the effect of the LGMDD1  
362 mutants is not independent of Hsp70 (at least for these substrates).

363 The function and interaction of the various Hsp40 domains have been studied  
364 extensively<sup>13,50</sup>. The efficiency of Hsp70 ATPase activity is heavily dependent on the proper  
365 functioning of the J and G/F domains of Hsp40<sup>50,51</sup>. Moreover, Hsp40 (Sis1) functions as a  
366 dimeric protein<sup>32</sup>. Interestingly, we found that LGMDD1 mutants show a diminished ability to  
367 form homodimers and heterodimers (with Sis1-WT). Thus, the LGMDD1 mutants show many  
368 defects that may contribute to perturbations in substrate processing.

369 Previously, it was suggested that the LGMDD1-causing mutations exert a deleterious  
370 dominant negative effect on the wild-type protein<sup>3</sup>. An excess of mutant (DNAJB6-F93L) to  
371 wild-type mRNA induced lethality in embryos, while an excess of wild-type to mutant mRNA  
372 gave rise to progressively increased rescue<sup>3</sup>. Consistent with this, we found that titrating Sis1-  
373 WT with an excess of LGMDD1 mutants (F106L and F115I) decreased ATPase activity.

374 Interaction of the Hsp70/40 machinery with a misfolded client is not sufficient to  
375 promote re-folding. The regulated cycle of client release and the potential for re-engagement is  
376 important, and this is dependent on nucleotide exchange. Indeed, changes in the availability or  
377 function of nucleotide exchange factors (NEFs) alone change client processing. Alterations in the  
378 NEF Sse1 were shown to alter yeast prion propagation in a strain-dependent manner<sup>52</sup>. Sse1 has  
379 been proposed to have multiple functions and can act as a disaggregase itself<sup>53,54</sup>. Our data  
380 suggest that the effect of the LGMDD1 mutants on the propagation of the [RNQ+] strain can be  
381 rescued by the deletion of Sse1 (HSP110). We also assessed the functional role of Sse1 in the  
382 rescue by using two Sse1 mutants; Sse1-K69Q and Sse1-G233D. We found a marked  
383 improvement in [RNQ+] prion propagation in yeast cells carrying these Sse1 mutants and  
384 harboring LGMDD1 mutants. Similarly, there was a considerable improvement in the refolding  
385 of luciferase activity in these cells. Notably, although the deletion of Sse1 alone showed partial  
386 improvement in [RNQ+] prion propagation in yeast cells, it did not show any difference in the  
387 refolding of luciferase, again perhaps indicating substrate specificity. Thus, this rescue further  
388 supports that the LGMDD1 mutants act in an Hsp70- dependent manner.

389 We hypothesize that the observed defects in the LGMDD1 mutants result in cellular  
390 phenotypes that are client-conformer specific. The Hsp70/DNAJ ATPase cycle is a process  
391 partitioned into two interconnected events; DNAJ is vital in the first half whereas NEFs play a  
392 significant role in the second half. Our data suggest that there are numerous defects associated  
393 with DNAJB6 (Sis1) mutants which result in either inhibition or delay in client processing in the  
394 first part of the Hsp70-ATPase cycle. Hsp70 has been shown to suppress proper substrate folding  
395 if it is not allowed to cycle off its client protein in various contexts<sup>55,56</sup>. Henceforth a longer  
396 interaction of LGMDD1 mutants with Hsp70 might lead to broader disruption of Hsp70-  
397 dependent processes, as this could titrate Hsp70 away from other clients<sup>57</sup>. Our data suggest that  
398 inhibiting the second half of the ATPase cycle, either by deletion or using Sse1 mutants, can  
399 have positive consequences on client processing. Interestingly, previous data suggest that the  
400 optimal NEF activity for protein disaggregation occurs at a reduced ratio of NEF:Hsp70 (1:10)<sup>58-</sup>  
401 <sup>60</sup>, and perhaps the deletion of Sse1 recapitulates such reduction in NEF activity in some manner  
402 (such as replacing the optimal NEF with another, such as Fes1). Moreover, the armadillo-type  
403 NEFs (budding yeast Fes1 and its human homolog HspBP1) employ flexible N-terminal release  
404 domains (RDs) with substrate-mimicking properties to ensure the efficient release of persistent  
405 substrates from Hsp70<sup>61</sup>. This is plausible due to the fact that NEFs perform dual functions:  
406 accelerating nucleotide exchange and securing Hsp70-liberated substrates. Of note, the high  
407 selectivity of exchange factors for their Hsp70 partner contributes to the functional heterogeneity  
408 of Hsp70 chaperone system<sup>62</sup>. These results indicate that fine-tuning of the two halves of the  
409 Hsp70 ATPase cycle involving LGMDD1 mutants and NEFs during the processing of its client  
410 proteins is critical (Fig. 8C). As such, we suggest that NEF inhibitors could provide a possible  
411 therapeutic strategy for the treatment of LGMDD1.

412

## 413 **Methodology**

### 414 **Cloning, Expression and Purification of Recombinant Proteins**

415 Sis1-WT, Sis1-mutants (F106L/N108L/D110Δ/F115I) and Ssa1-WT were cloned into pPROEx-  
416 Htb vector obtained from Addgene. The plasmid encodes a hexa-His-tag, a TEV cleavage site,  
417 and the respective cloned gene for expression. All Sis1 mutants were generated using the Quick  
418 Change Mutagenesis Kit (Agilent Technologies #200517). Primer sequences were generated

419 using Agilent's online primer design program. Mutagenesis was confirmed by sequencing the  
420 entire coding region of *SIS1*. Sis1-WT and Sis1-mutants were expressed at 16 °C, whereas Ssa1-  
421 WT was expressed at 18 °C to increase the fraction of soluble protein. All purification steps were  
422 carried out at 4 °C. Protein purity was more than 99% as determined by SDS/PAGE and  
423 Coomassie staining. Final protein concentration was estimated by Bradford assay, using bovine  
424 serum albumin as the standard. Following purification, all the proteins were frozen on liquid  
425 nitrogen and stored at -80 °C till further use. Sis1-WT and mutants were purified using standard  
426 protocol with some modifications. Briefly, these were purified from *Escherichia coli* strain Lemo  
427 21(DE3) (New England Biolabs) grown in 2X YT medium at 30 °C until  $OD_{600} = 0.6-0.8$ . The  
428 cultures were induced with 0.5 mM IPTG and grown overnight at 16 °C. Cells were harvested  
429 and lysed in buffer A (50 mM Sodium phosphate buffer (pH 7.4), 300 mM NaCl, 5 mM  $MgCl_2$ ,  
430 10 mM Imidazole, 0.1% Igepal, 0.01 M TCEP (tris(2-carboxyethyl)phosphine), protease  
431 inhibitor cocktail (EDTA-free from Roche) and a pinch of DNase I. Cell debris was cleared by  
432 centrifugation (20,000 g) and the supernatant loaded on cobalt-based Talon metal affinity resin.  
433 After washing, proteins were eluted as gradient fractions with buffer A containing increasing  
434 concentrations of imidazole (150 mM – 400 mM). Purified proteins were incubated with His-  
435 TEV (purified in the lab) protease at 30° for 1 h. The samples were extensively dialyzed at 4 °C  
436 and again passed through Talon metal affinity resin to remove the cleaved His tag and His-TEV  
437 protease. The pure proteins were concentrated and stored at -80 °C. Similarly, Ssa1-WT protein  
438 was also purified using an established procedure<sup>63</sup>. Briefly, protein was purified  
439 from *Escherichia coli* strain Rosetta 2(DE3) (Invitrogen) grown in LB medium with 300 mM  
440 NaCl at 30 °C until  $OD_{600} = 0.6-0.8$ . The culture was induced with 0.5 mM IPTG and grown  
441 overnight at 18 °C. Cells were harvested and lysed in buffer A (20 mM HEPES, 150 mM NaCl, 20  
442 mM  $MgCl_2$ , 20 mM KCl, protease inhibitor cocktail (EDTA-free from Roche)) using lysozyme.  
443 The rest of the protocol was similar to that of Sis1-WT and mutants, with only exception being  
444 that Ssa1-WT was eluted with buffer A containing 250 mM imidazole. Rnq1-WT full-length  
445 protein was purified exactly as described in previous publication from our lab<sup>26</sup>.

## 446 **Binding Assays**

447 **Substrate-binding ELISA assays** - This was performed as described earlier<sup>25</sup> with some  
448 modifications. Two different substrate proteins- Rnq1 and firefly luciferase (Promega

449 Corporation) were denatured for 1 h at 25 °C in a buffer comprising of 3 M guanidine HCl, 25  
450 mM HEPES (pH 7.5), 50 mM KCl, 5 mM MgCl<sub>2</sub>, and 5 mM DTT. Following denaturation,  
451 substrates were diluted in 0.1 M NaHCO<sub>3</sub> and bound to microtiter plate (CoStar 3590 EIA plates,  
452 Corning) at a concentration of 0.4 µg/well for Rnq1 and 0.1 µg/well for luciferase, respectively.  
453 Unbound substrate was removed by washing with phosphate buffered saline (PBS). Unreacted  
454 sites were blocked with 0.2 M glycine (100 µl/well) for 30 min at 24 °C, followed by washing  
455 with PBS-T (PBS containing 0.05% Tween 20). Non-specific binding was eliminated by  
456 blocking with 0.5% fatty-acid-free bovine serum albumin (BSA) (Millipore Sigma) in PBS for 6  
457 hours. The wells were subsequently washed with PBS-T. Sis1-WT and Sis1-mutants were  
458 serially diluted in PBST (substituted with 0.5% BSA) and incubated with substrate for overnight  
459 at 24 °C. After extensive washing with PBS-T, rabbit anti-Sis1 antibody (CosmoBio) at a  
460 dilution of (1:15000) was added and incubated for 2 h at 24 °C. This was followed by further  
461 washings and addition of donkey-anti-rabbit HRP-conjugated (Millipore Sigma) (1:4000) as  
462 secondary antibody. The amount of Sis1 retained was determined by developing a reaction using  
463 tetramethyl benzidine/H<sub>2</sub>O<sub>2</sub> (TMB peroxidase EIA substrate) kit (Bio-Rad). The colour was  
464 measured at 450 nm (SpectraMax M2e fluorimeter microplate reader) after terminating the  
465 reaction with 0.02 N H<sub>2</sub>SO<sub>4</sub>.

466 *Ssa1-binding assays* - Ssa1 (200 nM) was immobilized in microtiter plate wells and dilutions of  
467 purified Sis1-WT and Sis1-mutants were incubated with it. Bound Sis1 was detected as  
468 described above.

469 ***Substrate bound Sis1 combined with Ssa1 binding assays*** – Denatured substrates (Rnq1 and  
470 luciferase) at a concentration of 0.4 ug/well and 0.1 ug/well, respectively, were mixed with Sis1-  
471 WT and Sis-mutant proteins (5 nM) and incubated for 1 h at 24 °C, prior to being adsorbed in the  
472 microtiter well plates. Following the steps of incubations, washings and blocking, serially diluted  
473 Ssa1-WT was added to each well. Subsequently, the wells were probed with rabbit-Ssa1  
474 antibody (1:2000) (Abcam), followed by mouse anti-rabbit HRP conjugated secondary antibody  
475 (Millipore Sigma). The detection method used was similar to that described above for detecting  
476 Sis1.

477 ***Homo/Hetero dimeric nature of Sis1 determining binding assays*** – Serially diluted His-tagged  
478 cleaved Sis1-WT and Sis1-mutants were adsorbed in the microtiter well plates. Following  
479 washings, serially diluted uncleaved His-tagged Sis1-WT and Sis1-mutants were added to the

480 wells in the following combinations [(Cleaved mutants + Uncleaved mutants =Homodimer);  
481 (Cleaved mutants + Uncleaved Sis1-WT = Heterodimer) along with appropriate controls for the  
482 assay. This was followed by washings, blocking and addition of mouse anti-His antibody  
483 (1:5000) (Invitrogen). Rabbit anti-mouse HRP conjugated antiserum (1:4000) (Millipore Sigma)  
484 was used as secondary antibody. The detection method was similar to that described above.

#### 485 **Amyloid Fiber Formation and Thioflavin T kinetics**

486 Purified Rnq1 was resuspended in 7 M guanidine hydrochloride and the protein concentration  
487 was determined. Rnq1 fibers were formed at 18°C, 25°C and 37°C with a starting monomer  
488 concentration of 8  $\mu$ M in Fiber-formation buffer (FFB) (50 mM KPO<sub>4</sub>, 2 M Urea, 150 mM NaCl,  
489 pH 6). For the seeded kinetics experiments, the fibers were seeded using 5% (w/w) seed. The  
490 fiber formation and kinetics assays were performed in the presence of Thioflavin T dye and acid-  
491 washed glass beads (Sigma) for agitation as described earlier<sup>26</sup>. Kinetic assays of fiber formation  
492 were done in a SpectraMax M2e fluorimeter microplate reader. The change in Thioflavin-T  
493 fluorescence over time was measured using an excitation wavelength of 450 nm and emission  
494 wavelength of 481 nm.

#### 495 **Colorimetric determination of ATPase activity**

496 The ATPase assay was performed as described before<sup>64</sup> with some modifications. Briefly, the  
497 ATPase reagent was made by combining 0.081% W/V Malachite Green with 2.3% W/V poly-  
498 vinyl alcohol, 5.7% W/V ammonium heptamolybdate in 6 M HCl, and water in 2:1:1:2 ratios (all  
499 purchased from Sigma with no further purification). This ATPase reagent was freshly prepared  
500 every day and was left standing for 2 h to get a stable green/golden solution, which was filtered  
501 through 0.45  $\mu$ m syringe filters (Millipore Sigma) before use. ATPase activity in the absence of  
502 any client protein was tested by incubating Sis1-WT/mutants, Ssa1-WT in the ratio of (0.05:1.0  
503  $\mu$ M) with 1 mM ATP, in assay buffer (0.02% Triton X-100, 40 mM Tris-HCl, 175 mM NaCl,  
504 and 5 mM MgCl<sub>2</sub>, pH 7.5) at 37 °C for different time-intervals as indicated in the figure legends.  
505 At the end of incubation 25  $\mu$ L of the reaction was added to a well in a 96 well plate, followed  
506 by 800 $\mu$ L of the ATPase reagent and 100  $\mu$ L of 34% sodium citrate to halt any further ATP  
507 hydrolysis. The mixture was allowed to incubate for 30 min at 24 °C before absorbance at 620  
508 nm was measured using a SpectraMax M2e fluorimeter microplate reader. A sample of ATP

509 alone in buffer was treated exactly the same and was subtracted from the sample absorbance to  
510 account for intrinsic ATP hydrolysis. To account for variability in measurements a phosphate  
511 standard curve (using potassium phosphate) was created for each day of measurements. For  
512 ATPase activity in presence of client proteins, the same procedure was followed with only  
513 exception being the addition of client protein Rnq1 monomer (25  $\mu$ M) and Rnq1 seeds (10% of  
514 which is used in final reaction) formed at three different temperatures (18°C, 25°C and 37°C)  
515 with the chaperones and ATP for incubation.

### 516 **Luciferase refolding assay**

517 Heat denatured refolding of luciferase was performed as previously described<sup>65</sup>. Briefly, Ssa1 (2  
518  $\mu$ M) were incubated in refolding buffer (50mM Tris pH 7.4, 150 mM KCl, 5 mM MgCl<sub>2</sub>)  
519 supplemented with 1 mM ATP and an ATP regenerating system (10 mM phosphocreatine, 100  
520 mg/ml phosphocreatine kinase) for 15 min at room temperature. Next, luciferase (25 nM) was  
521 added and incubated for a further 10 min. Then Sis1-WT/mutants (0.05  $\mu$ M) was added and the  
522 mixture was heat shocked at 44 °C for 20 min. The reactions were then immediately moved to  
523 room temperature. Finally, 25  $\mu$ L aliquots of the refolding reaction were then taken and added to  
524 50  $\mu$ L of luciferase assay reagent (Promega Corporation). At various time points, activity was  
525 then measured with a GloMax Luminometer (Promega Corporation).

### 526 **Titration assays**

527 All the assays were performed by titrating the concentration of Sis1-mutants (F106L and F115I)  
528 with Sis1-WT such that the total concentration of protein was the same as been used individually  
529 across different assays.

### 530 **Yeast strains, plasmids and Transformation**

531 The yeast strains used in this study are derived from *Saccharomyces cerevisiae* 74-D694 (*ade1-*  
532 *14 his3- $\Delta$ 200 leu2-3, 112 trp1-289 ura 3-52*). Yeast cells were grown and manipulated using  
533 standard techniques<sup>66</sup>. As indicated, cells were grown in rich media YPD (1% yeast extract, 2%  
534 peptone, 2% dextrose) or in synthetic defined (SD) media (0.67% yeast nitrogen base without  
535 amino acids, 2% dextrose) lacking specific nutrients to select for appropriate plasmids. Wild-  
536 type (WT) yeast harboring the s. d. medium [*RNQ+*] variant and the [*rnq-*] control strain were

537 kindly provided by Dr. Susan Liebman (University of Nevada, Reno, Nevada, USA)<sup>67</sup>.  
538 Construction of  $\Delta$ *Sis1* [*rnq-*] and s. d. medium [*RNQ+*] yeast strains were described previously<sup>12</sup>.  
539  $\Delta$ *Sse1* and all other delta strains in s. d. medium [*RNQ+*] background were created using the  
540 standard protocol. Medium containing 1mg/mL 5-fluoroorotic acid (5-FOA) that selects against  
541 cells maintaining *URA3*- marked plasmids was used to replace WT *Sis1* with the mutant  
542 constructs using the plasmid shuffle technique. Plasmid transformations were done using  
543 polyethylene-glycol/lithium-acetate (PEG/LioAC) technique and the cells were selected using  
544 SD-trp/his plates.

545 Plasmid pRS316-*SIS1* was kindly provided by Dr. Elizabeth Craig (University of Wisconsin,  
546 Madison, Madison, Wisconsin, USA)<sup>22</sup>. Plasmids pRS414-*Sse1-K69Q*, and pRS414-*Sse1-*  
547 *G233D* were kind gifts from Dr. Kevin Morano (McGovern Medical School, UT Health,  
548 Houston, Texas, USA)<sup>37</sup>. Construction of pRS314-*Sis1* and LGMDD1 mutants were described  
549 previously. Using the standard molecular techniques we constructed p413TEF-*Sse1-K69Q* and  
550 p413TEF-*Sse1-G233D*. Plasmid pRS316-GPD-Lux was a kind gift from Dr. Bernd Bukau  
551 (Center for Molecular Biology of Heidelberg University, Heidelberg, Germany)<sup>39</sup>.

## 552 **Protein fiber Transformation for Phenotypic analysis**

553 Transformation of Rnq1 fibers into a [*rnq-*] 74-D694 (*ade1-14, ura3-52, leu2-3,112, trp1-289,*  
554 *his3-200, sup35::RRP*) yeast strain in the presence and absence of *Sis1*-WT/ mutants was  
555 conducted as described<sup>68</sup>. The resulting colonies formed after infecting fibers formed in vitro in  
556 the presence and absence of chaperones were replica plated onto rich medium (YPD) plates to  
557 assay for colony color. Colonies that appeared to have acquired the prion state by nonsense  
558 suppression were picked and spotted on YPD, YPD containing 3 mM GdnHCl, and SD-Ade for  
559 phenotypic analyses.

## 560 **Protein Analysis**

561 Yeast samples were lysed with glass beads in buffer (100 mM Tris-HCl pH7.5, 200mM NaCl,  
562 1mM EDTA, 5% glycerol, 0.5 mM DTT, 3 mM PMSF, 50 mM N-ethylmaleimide (NEM),  
563 complete protease inhibitor from Roche) and pre-cleared at 6000 rpm for 15 sec. Protein  
564 concentration of cells lysates was then normalized. For well-trap assays, samples were incubated  
565 at room temperature or 100°C in sample buffer (200mM Tris-HCl pH 6.8, 4% SDS, 0.4%

566 bromophenol blue, 40% glycerol), then analyzed by SD-PAGE and western blot using an  $\alpha$ Rnq1  
567 antibody. Boiled gel assays were performed as described previously<sup>15</sup>. Briefly, yeast cells were  
568 lysed with glass beads in buffer (25mM Tris-HCl pH7.5, 100mM NaCl, 1mM EDTA, protease  
569 inhibitors) and pre-cleared at 6,000 rpm for 1 minute at 4°C. Protein concentration of cell lysates  
570 was normalized using a Bradford assay and mixed with SDS-Page sample buffer (200mM Tris-  
571 HCl pH 6.8, 4% SDS, 0.4% bromophenol blue, 40% glycerol). Samples remained un-boiled and  
572 were loaded on a 12% polyacrylamide gel and run under constant current of 110V until the dye  
573 front migrated halfway through the resolving gel. The current was then stopped, and the gel in  
574 glass plates was sealed in plastic and boiled upright for 15 mins in a 95-100°C water bath. After  
575 boiling, gels were removed from the plastic cover and were reinserted in the SDS-PAGE  
576 apparatus, where voltage was re-applied until the dye migrated to the bottom of the gel. SDS-  
577 PAGE was followed by standard western blotting with  $\alpha$ Rnq1 antibody. Semi-denaturing agarose  
578 gel electrophoresis (SDD-AGE) for [RNQ+] fibers was performed as previously described<sup>69</sup>.

#### 579 **Negative Staining Transmission Electron Microscopy**

580 Rnq1 fibers were generated as described above. Negative staining of Rnq1 samples was  
581 performed by depositing 8uL of sample and incubating for one minute on carbon coated 200  
582 mesh copper grids (01840-F, Ted Pella, Redding, CA), held by forceps carbon side up which had  
583 been freshly glow discharged for 30 seconds in a Solarus 950 plasma cleaner (Gatan, Pleasanton,  
584 CA). Post-incubation, each grid was washed five times in separate ultrapure water droplets and  
585 subsequently stained with 0.75% uranyl formate for 2 minutes. Excess uranyl formate was  
586 blotted off using filter paper (Whatman No.2, Fisher Scientific, Hampton, NH) and subsequently  
587 air dried. Sample grids were imaged using a JEOL JEM-1400 Plus Transmission Electron  
588 Microscope operating at an accelerating voltage of 120 kV equipped with an NanoSprint15  
589 MKII sCMOS camera (AMT Imaging, Woburn, MA). Images were acquired using a total  
590 exposure time of 5 seconds containing ten 500ms drift frames which were subsequently aligned  
591 and averaged using the AMT ImageCapture Engine acquisition software at nominal  
592 magnifications ranging between 20,000-50,000x.

#### 593 **Statistical analysis**

594 Error bars represent standard error mean from at least three experiments. Significance was  
595 determined for two-sample comparisons using the unpaired *t*-test function with a threshold of  
596 two-tailed *p* values less than 0.05 for \*, 0.01 for \*\* and 0.001 for \*\*\*.

597

598

## 599 **References**

- 600 1. Iyadurai, S. J. P. & Kissel, J. T. The Limb-Girdle Muscular Dystrophies and the Dystrophinopathies.  
601 *Continuum (Minneap Minn)* **22**, 1954–1977 (2016).
- 602 2. Kley, R. A., Olivé, M. & Schröder, R. New aspects of myofibrillar myopathies. *Curr Opin Neurol*  
603 **29**, 628–634 (2016).
- 604 3. Sarparanta, J. *et al.* Mutations affecting the cytoplasmic functions of the co-chaperone DNAJB6  
605 cause limb-girdle muscular dystrophy. *Nat Genet* **44**, 450–455, S1-2 (2012).
- 606 4. Harms, M. B. *et al.* Exome sequencing reveals DNAJB6 mutations in dominantly-inherited  
607 myopathy. *Ann Neurol* **71**, 407–416 (2012).
- 608 5. Ruggieri, A. *et al.* Complete loss of the DNAJB6 G/F domain and novel missense mutations cause  
609 distal-onset DNAJB6 myopathy. *Acta Neuropathol Commun* **3**, 44 (2015).
- 610 6. Palmio, J. *et al.* Novel mutations in DNAJB6 gene cause a very severe early-onset limb-girdle  
611 muscular dystrophy 1D disease. *Neuromuscul Disord* **25**, 835–842 (2015).
- 612 7. Sato, T. *et al.* DNAJB6 myopathy in an Asian cohort and cytoplasmic/nuclear inclusions.  
613 *Neuromuscul Disord* **23**, 269–276 (2013).
- 614 8. Hageman, J. *et al.* A DNAJB chaperone subfamily with HDAC-dependent activities suppresses  
615 toxic protein aggregation. *Mol Cell* **37**, 355–369 (2010).
- 616 9. Watson, E. D., Geary-Joo, C., Hughes, M. & Cross, J. C. The Mrj co-chaperone mediates keratin  
617 turnover and prevents the formation of toxic inclusion bodies in trophoblast cells of the placenta.  
618 *Development* **134**, 1809–1817 (2007).
- 619 10. Zhang, Y. *et al.* The Hsp40 family chaperone protein DnaJB6 enhances Schlafen1 nuclear  
620 localization which is critical for promotion of cell-cycle arrest in T-cells. *Biochem J* **413**, 239–250 (2008).
- 621 11. Mitra, A., Menezes, M. E., Shevde, L. A. & Samant, R. S. DNAJB6 induces degradation of beta-  
622 catenin and causes partial reversal of mesenchymal phenotype. *J Biol Chem* **285**, 24686–24694 (2010).

- 623 12. Stein, K. C., Bengoechea, R., Harms, M. B., Wehl, C. C. & True, H. L. Myopathy-causing mutations  
624 in an HSP40 chaperone disrupt processing of specific client conformers. *J Biol Chem* **289**, 21120–21130  
625 (2014).
- 626 13. Kampinga, H. H. & Craig, E. A. The HSP70 chaperone machinery: J proteins as drivers of  
627 functional specificity. *Nat Rev Mol Cell Biol* **11**, 579–592 (2010).
- 628 14. Rose, J. M., Novoselov, S. S., Robinson, P. A. & Cheetham, M. E. Molecular chaperone-mediated  
629 rescue of mitophagy by a Parkin RING1 domain mutant. *Hum Mol Genet* **20**, 16–27 (2011).
- 630 15. Pullen, M. Y., Wehl, C. C. & True, H. L. Client processing is altered by novel myopathy-causing  
631 mutations in the HSP40 J domain. *PLoS One* **15**, e0234207 (2020).
- 632 16. Frost, B. & Diamond, M. I. Prion-like mechanisms in neurodegenerative diseases. *Nat Rev*  
633 *Neurosci* **11**, 155–159 (2010).
- 634 17. Glover, J. R. & Lindquist, S. Hsp104, Hsp70, and Hsp40: a novel chaperone system that rescues  
635 previously aggregated proteins. *Cell* **94**, 73–82 (1998).
- 636 18. True, H. L. The battle of the fold: chaperones take on prions. *Trends Genet* **22**, 110–117 (2006).
- 637 19. Satpute-Krishnan, P., Langseth, S. X. & Serio, T. R. Hsp104-dependent remodeling of prion  
638 complexes mediates protein-only inheritance. *PLoS Biol* **5**, e24 (2007).
- 639 20. Collinge, J. & Clarke, A. R. A general model of prion strains and their pathogenicity. *Science* **318**,  
640 930–936 (2007).
- 641 21. Palmio, J. *et al.* Mutations in the J domain of DNAJB6 cause dominant distal myopathy.  
642 *Neuromuscul Disord* **30**, 38–46 (2020).
- 643 22. Lopez, N., Aron, R. & Craig, E. A. Specificity of class II Hsp40 Sis1 in maintenance of yeast prion  
644 [RNQ+]. *Mol Biol Cell* **14**, 1172–1181 (2003).
- 645 23. Vitrenko, Y. A., Gracheva, E. O., Richmond, J. E. & Liebman, S. W. Visualization of aggregation of  
646 the Rnq1 prion domain and cross-seeding interactions with Sup35NM. *J Biol Chem* **282**, 1779–1787  
647 (2007).
- 648 24. Naiki, H. & Gejyo, F. Kinetic analysis of amyloid fibril formation. *Methods Enzymol* **309**, 305–318  
649 (1999).
- 650 25. Aron, R., Lopez, N., Walter, W., Craig, E. A. & Johnson, J. In vivo bipartite interaction between  
651 the Hsp40 Sis1 and Hsp70 in *Saccharomyces cerevisiae*. *Genetics* **169**, 1873–1882 (2005).
- 652 26. Kalastavadi, T. & True, H. L. Analysis of the [RNQ+] prion reveals stability of amyloid fibers as the  
653 key determinant of yeast prion variant propagation. *J Biol Chem* **285**, 20748–20755 (2010).

- 654 27. Yan, W. & Craig, E. A. The glycine-phenylalanine-rich region determines the specificity of the  
655 yeast Hsp40 Sis1. *Mol Cell Biol* **19**, 7751–7758 (1999).
- 656 28. Perales-Calvo, J., Muga, A. & Moro, F. Role of DnaJ G/F-rich domain in conformational  
657 recognition and binding of protein substrates. *J Biol Chem* **285**, 34231–34239 (2010).
- 658 29. Sondheimer, N., Lopez, N., Craig, E. A. & Lindquist, S. The role of Sis1 in the maintenance of the  
659 [RNQ+] prion. *EMBO J* **20**, 2435–2442 (2001).
- 660 30. Wawrzynów, A. & Zylicz, M. Divergent effects of ATP on the binding of the DnaK and DnaJ  
661 chaperones to each other, or to their various native and denatured protein substrates. *J Biol Chem* **270**,  
662 19300–19306 (1995).
- 663 31. Bengoechea, R. *et al.* Inhibition of DNAJ-HSP70 interaction improves strength in muscular  
664 dystrophy. *J. Clin. Invest.* (2020) doi:10.1172/JCI136167.
- 665 32. Li, J., Qian, X. & Sha, B. Heat shock protein 40: structural studies and their functional  
666 implications. *Protein Pept Lett* **16**, 606–612 (2009).
- 667 33. Sha, B., Lee, S. & Cyr, D. M. The crystal structure of the peptide-binding fragment from the yeast  
668 Hsp40 protein Sis1. *Structure* **8**, 799–807 (2000).
- 669 34. Abrams, J. L., Verghese, J., Gibney, P. A. & Morano, K. A. Hierarchical functional specificity of  
670 cytosolic heat shock protein 70 (Hsp70) nucleotide exchange factors in yeast. *J Biol Chem* **289**, 13155–  
671 13167 (2014).
- 672 35. Yakubu, U. M. & Morano, K. A. Roles of the nucleotide exchange factor and chaperone Hsp110  
673 in cellular proteostasis and diseases of protein misfolding. *Biol Chem* **399**, 1215–1221 (2018).
- 674 36. Shaner, L., Sousa, R. & Morano, K. A. Characterization of Hsp70 binding and nucleotide exchange  
675 by the yeast Hsp110 chaperone Sse1. *Biochemistry* **45**, 15075–15084 (2006).
- 676 37. Shaner, L., Trott, A., Goeckeler, J. L., Brodsky, J. L. & Morano, K. A. The function of the yeast  
677 molecular chaperone Sse1 is mechanistically distinct from the closely related hsp70 family. *J Biol Chem*  
678 **279**, 21992–22001 (2004).
- 679 38. Tipton, K. A., Verges, K. J. & Weissman, J. S. In vivo monitoring of the prion replication cycle  
680 reveals a critical role for Sis1 in delivering substrates to Hsp104. *Mol Cell* **32**, 584–591 (2008).
- 681 39. Tessarz, P., Mogk, A. & Bukau, B. Substrate threading through the central pore of the Hsp104  
682 chaperone as a common mechanism for protein disaggregation and prion propagation. *Mol Microbiol*  
683 **68**, 87–97 (2008).
- 684 40. Smith, D. A., Carland, C. R., Guo, Y. & Bernstein, S. I. Getting folded: chaperone proteins in  
685 muscle development, maintenance and disease. *Anat Rec (Hoboken)* **297**, 1637–1649 (2014).

- 686 41. Stein, K. C. & True, H. L. Extensive diversity of prion strains is defined by differential chaperone  
687 interactions and distinct amyloidogenic regions. *PLoS Genet* **10**, e1004337 (2014).
- 688 42. Vaquer-Alicea, J. & Diamond, M. I. Propagation of Protein Aggregation in Neurodegenerative  
689 Diseases. *Annu Rev Biochem* **88**, 785–810 (2019).
- 690 43. Caughey, B. & Kraus, A. Transmissibility versus Pathogenicity of Self-Propagating Protein  
691 Aggregates. *Viruses* **11**, E1044 (2019).
- 692 44. Sanders, D. W. *et al.* Distinct tau prion strains propagate in cells and mice and define different  
693 tauopathies. *Neuron* **82**, 1271–1288 (2014).
- 694 45. Mirbaha, H. *et al.* Inert and seed-competent tau monomers suggest structural origins of  
695 aggregation. *Elife* **7**, e36584 (2018).
- 696 46. Sharma, A. M., Thomas, T. L., Woodard, D. R., Kashmer, O. M. & Diamond, M. I. Tau monomer  
697 encodes strains. *Elife* **7**, e37813 (2018).
- 698 47. Deane, C. A. S. & Brown, I. R. Components of a mammalian protein disaggregation/refolding  
699 machine are targeted to nuclear speckles following thermal stress in differentiated human neuronal  
700 cells. *Cell Stress Chaperones* **22**, 191–200 (2017).
- 701 48. Beissinger, M. & Buchner, J. How chaperones fold proteins. *Biol Chem* **379**, 245–259 (1998).
- 702 49. Faust, O. *et al.* HSP40 proteins use class-specific regulation to drive HSP70 functional diversity.  
703 *Nature* **587**, 489–494 (2020).
- 704 50. Rosenzweig, R., Nillegoda, N. B., Mayer, M. P. & Bukau, B. The Hsp70 chaperone network. *Nat*  
705 *Rev Mol Cell Biol* **20**, 665–680 (2019).
- 706 51. Kampinga, H. H. *et al.* Function, evolution, and structure of J-domain proteins. *Cell Stress*  
707 *Chaperones* **24**, 7–15 (2019).
- 708 52. Fan, Q., Park, K.-W., Du, Z., Morano, K. A. & Li, L. The role of Sse1 in the de novo formation and  
709 variant determination of the [PSI<sup>+</sup>] prion. *Genetics* **177**, 1583–1593 (2007).
- 710 53. Shorter, J. The mammalian disaggregase machinery: Hsp110 synergizes with Hsp70 and Hsp40 to  
711 catalyze protein disaggregation and reactivation in a cell-free system. *PLoS One* **6**, e26319 (2011).
- 712 54. Sadlish, H. *et al.* Hsp110 chaperones regulate prion formation and propagation in *S. cerevisiae*  
713 by two discrete activities. *PLoS One* **3**, e1763 (2008).
- 714 55. Kirschke, E., Goswami, D., Southworth, D., Griffin, P. R. & Agard, D. A. Glucocorticoid receptor  
715 function regulated by coordinated action of the Hsp90 and Hsp70 chaperone cycles. *Cell* **157**, 1685–1697  
716 (2014).

- 717 56. Sekhar, A., Santiago, M., Lam, H. N., Lee, J. H. & Cavagnero, S. Transient interactions of a slow-  
718 folding protein with the Hsp70 chaperone machinery. *Protein Sci* **21**, 1042–1055 (2012).
- 719 57. Park, S.-H. *et al.* PolyQ proteins interfere with nuclear degradation of cytosolic proteins by  
720 sequestering the Sis1p chaperone. *Cell* **154**, 134–145 (2013).
- 721 58. Yakubu, U. M. & Morano, K. A. Suppression of aggregate and amyloid formation by a novel  
722 intrinsically disordered region in metazoan Hsp110 chaperones. *J Biol Chem* **296**, 100567 (2021).
- 723 59. Dragovic, Z., Broadley, S. A., Shomura, Y., Bracher, A. & Hartl, F. U. Molecular chaperones of the  
724 Hsp110 family act as nucleotide exchange factors of Hsp70s. *EMBO J* **25**, 2519–2528 (2006).
- 725 60. Wentink, A. S. *et al.* Molecular dissection of amyloid disaggregation by human HSP70. *Nature*  
726 **587**, 483–488 (2020).
- 727 61. Gowda, N. K. C. *et al.* Nucleotide exchange factors Fes1 and HspBP1 mimic substrate to release  
728 misfolded proteins from Hsp70. *Nat Struct Mol Biol* **25**, 83–89 (2018).
- 729 62. Brehmer, D. *et al.* Tuning of chaperone activity of Hsp70 proteins by modulation of nucleotide  
730 exchange. *Nat Struct Biol* **8**, 427–432 (2001).
- 731 63. Sharma, D. & Masison, D. C. Single methyl group determines prion propagation and protein  
732 degradation activities of yeast heat shock protein (Hsp)-70 chaperones Ssa1p and Ssa2p. *Proc Natl Acad*  
733 *Sci U S A* **108**, 13665–13670 (2011).
- 734 64. Chang, L. *et al.* High-throughput screen for small molecules that modulate the ATPase activity of  
735 the molecular chaperone DnaK. *Anal Biochem* **372**, 167–176 (2008).
- 736 65. Lindstedt, P. R. *et al.* Enhancement of the Anti-Aggregation Activity of a Molecular Chaperone  
737 Using a Rationally Designed Post-Translational Modification. *ACS Cent Sci* **5**, 1417–1424 (2019).
- 738 66. Gietz, D., St Jean, A., Woods, R. A. & Schiestl, R. H. Improved method for high efficiency  
739 transformation of intact yeast cells. *Nucleic Acids Res* **20**, 1425 (1992).
- 740 67. Bradley, M. E., Edskes, H. K., Hong, J. Y., Wickner, R. B. & Liebman, S. W. Interactions among  
741 prions and prion ‘strains’ in yeast. *Proc Natl Acad Sci U S A* **99 Suppl 4**, 16392–16399 (2002).
- 742 68. Tanaka, M. & Weissman, J. S. An efficient protein transformation protocol for introducing prions  
743 into yeast. *Methods Enzymol* **412**, 185–200 (2006).
- 744 69. Bardill, J. P. & True, H. L. Heterologous prion interactions are altered by mutations in the prion  
745 protein Rnq1p. *J Mol Biol* **388**, 583–596 (2009).
- 746 70. Vitrenko, Y. A., Pavon, M. E., Stone, S. I. & Liebman, S. W. Propagation of the [PIN+] prion by  
747 fragments of Rnq1 fused to GFP. *Curr Genet* **51**, 309–319 (2007).

749

## 750 **Acknowledgements**

751 We are thankful to S. Liebman, J. Weissman, K. Morano, and E. Craig for plasmids and strains. We also  
752 thank Kevin Stein for initial experiments with Sse1. We are thankful to Patrick McConnell and Kevin M.  
753 Kaltenbronn for helping with protein purification and luciferase assay, respectively. We are thankful to  
754 members of True lab and Wehl lab for helpful discussions and comments on the manuscript. This work  
755 was supported by: National Institutes of Health Grant R01AR068797 to HLT and CCW. The funders had  
756 no role in study design, data collection and analysis, decision to publish, or preparation of the manuscript.

## 757 **Author contributions**

758 A.K.B., C.C.W., and H.L.T. conceived and designed the experiments and analyzed data. A.K.B.  
759 performed all the experiments and wrote the initial draft. M.J.R. and J.A.J.F collected the negative-  
760 staining TEM images. J.A.D. performed the site-directed mutagenesis. A.K.B., C.C.W., and H.L.T.  
761 reviewed and edited the manuscript. All authors provided editorial input.

## 762 **Competing interests**

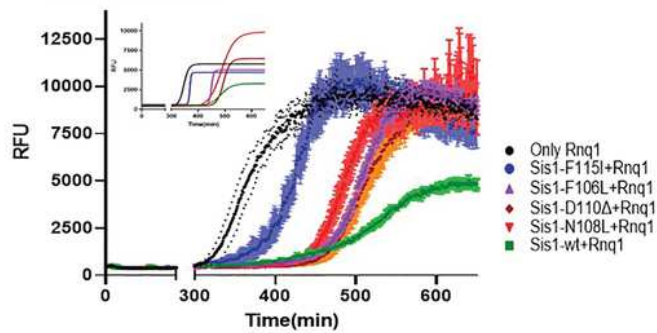
763 The authors declare no competing interests.

764

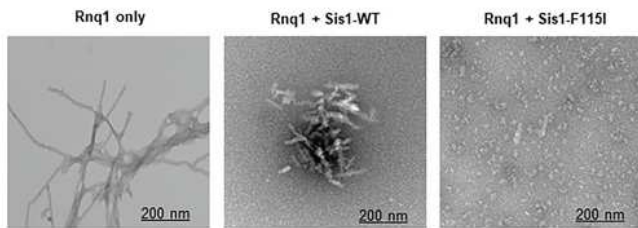
# Figures

Figure 1

**A. ThT Kinetics of Unseeded Rnq1 in presence of LGMDD1 mutants**



**B. Negative stain TEM images**



**C. Refolding activity of heat-denatured luciferase in presence of LGMDD1 mutants**

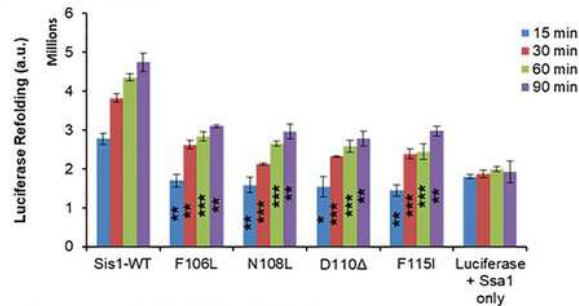


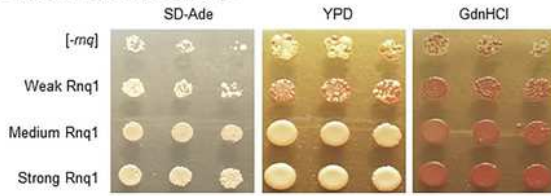
Figure 1. **LGMD1 G/F domain mutants show variability in substrate processing.** (A) Kinetics of Rnq1 fibrillation in the presence of unseeded Rnq1 only (**black**), Sis1-WT (**green**), Sis1-F106L (**purple**), Sis1-N108L (**red**), Sis1-D110Δ (**brown**), or Sis1-F115I (**blue**) measured by ThT fluorescence assay. *Inset*:- Fitted graph using the aggregation kinetics equation  $y=y_i+mx_i+(y_f+mx_f)/1+(e^{-x/τ})$  where  $(y_i + mx_i)$  is the initial line,  $(y_f + mx_f)$  is the final line, and  $x_0$  is the midpoint of the maximum signal. (B) The morphology of amyloid fibers formed from Rnq1 at 18°C in vitro in the presence and absence of Sis1-WT and/or LGMD1 mutant were imaged by TEM. The scale bar represents 200 nm. (C) Refolding activity of heat-denatured luciferase in the presence of LGMD1 mutants. Luciferase along with Ssa1-WT and Sis1-WT/mutants was incubated at 42°C for 10 min to heat denature luciferase. At various time points, activity was measured by a luminometer after adding substrate. Each LGMD1 mutant was compared with Sis1-WT across all time-points. \*\*\* $p < 0.001$ , \*\* $p < 0.01$ , and \* $p < 0.05$ .

Figure 1

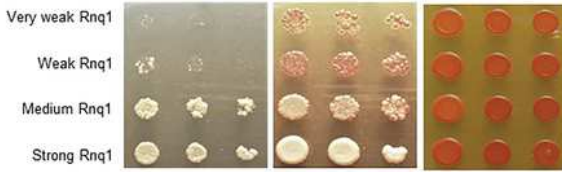
See figure for legend.

Figure 2

A. RNQ1 variant controls



B. RNQ1 variants in presence of Rnq1 fibers and LGMDD1 mutants



C. Graph showing difference in RNQ1 variants formation with LGMDD1 mutants

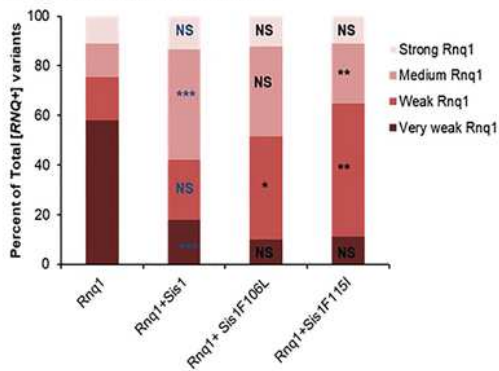


Figure 2. **Phenotypic distribution of [RNQ+] strain alters with LGMDD1 G/F domain mutants.** Transformation of Rnq1 amyloid fibers formed at 18°C into [*rnq*-] 74D-694 yeast cells induces strains of the [RNQ+] prion (A). RRP was used to assess [RNQ+] phenotype. [RNQ+] prion strains co-aggregate with RRP and cause different phenotypes; colony color on YPD and growth on SD-ade medium are indicative of different levels of suppression of the *ade1-14* premature stop codon to produce Ade1 and represent different [RNQ+] strains. Curability by growth and color on medium containing GdnHCl was used to determine prion-dependence of phenotypes. The transformants from five separate experiments for each sample set were picked and >200 colonies for each set were scored as very weak, weak, medium, or strong [RNQ+] (B) and graphed for statistical analysis (C). In panel (C), the blue color indicates the comparison between Rnq1 (alone) and Rnq1 with Sis1-WT, black color indicates the comparison between Sis1-WT and LGMDD1 mutants (F106L and F115I). \*\*\**p*<0.001, \*\**p*<0.01, \**p*<0.05, and NS is non-significant.

Figure 2

See figure for legend.

Figure 3

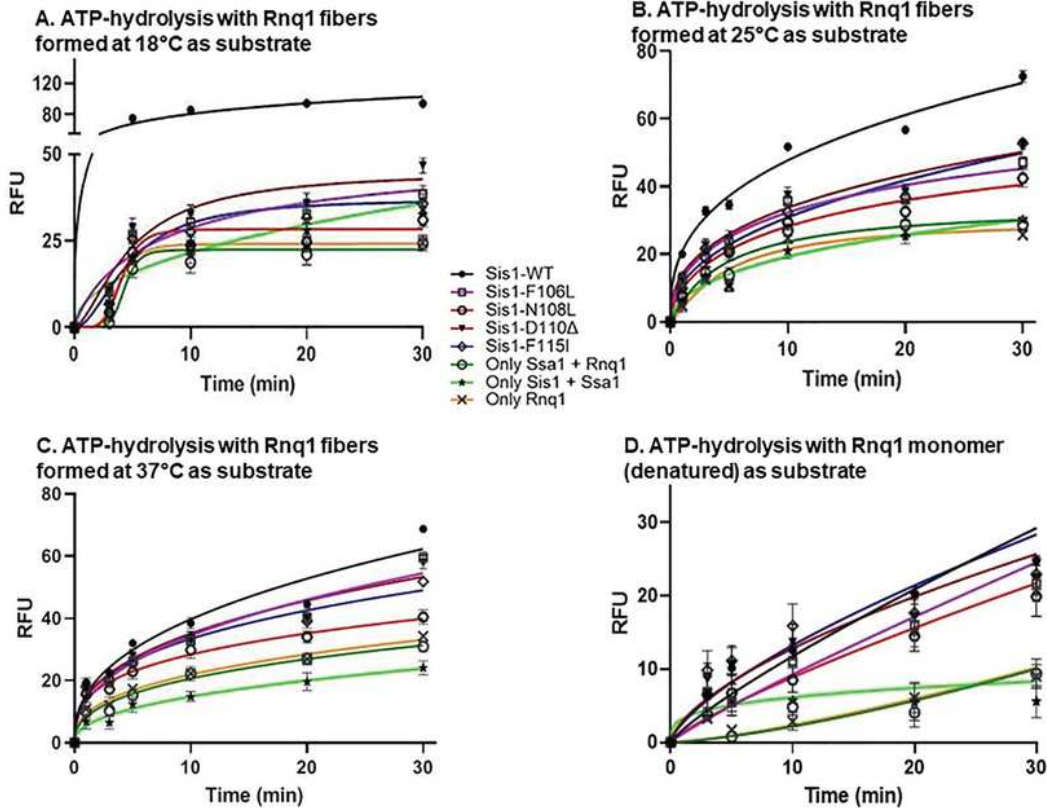


Figure 3. **Stimulation of ATPase activity of Ssa1 by LGMDD1 G/F domain mutants is client-conformation specific.** Stimulation of Ssa1 ATPase activity in the presence of Rnq1 seeds formed at (A) 18°C, (B) 25°C, and (C) 37°C, and (D) Rnq1 monomer. Ssa1 (1 μM) in complex with ATP (1 mM) in the presence of Sis1-WT (**black**) or Sis1-mutants (Sis1-F106L (**purple**), Sis1-N108L (**red**), Sis1-D110Δ (**brown**), or Sis1-F115I (**blue**)) (0.05 μM). The fraction of ATP converted to ADP was determined at indicated times. For (A), (B), and (C) a total of 10% seeds were used in a reaction. For (D) Rnq1 monomer used was 25 μM. In all cases, only Rnq1 (**orange**), Sis1 with Ssa1 (**light green**) and Ssa1 with Rnq1 (**dark green**) were used as controls. For A-D, Sis1-WT was compared with LGMDD1- mutants at all time points. Here we show the significant difference at one time-point (20 min). For (A) and (B) values were \*\*\* $p < 0.001$ , for (C) values were \*\* $p < 0.01$ , for (D) values were non-significant (NS).

Figure 3

See figure for legend.

Figure 4

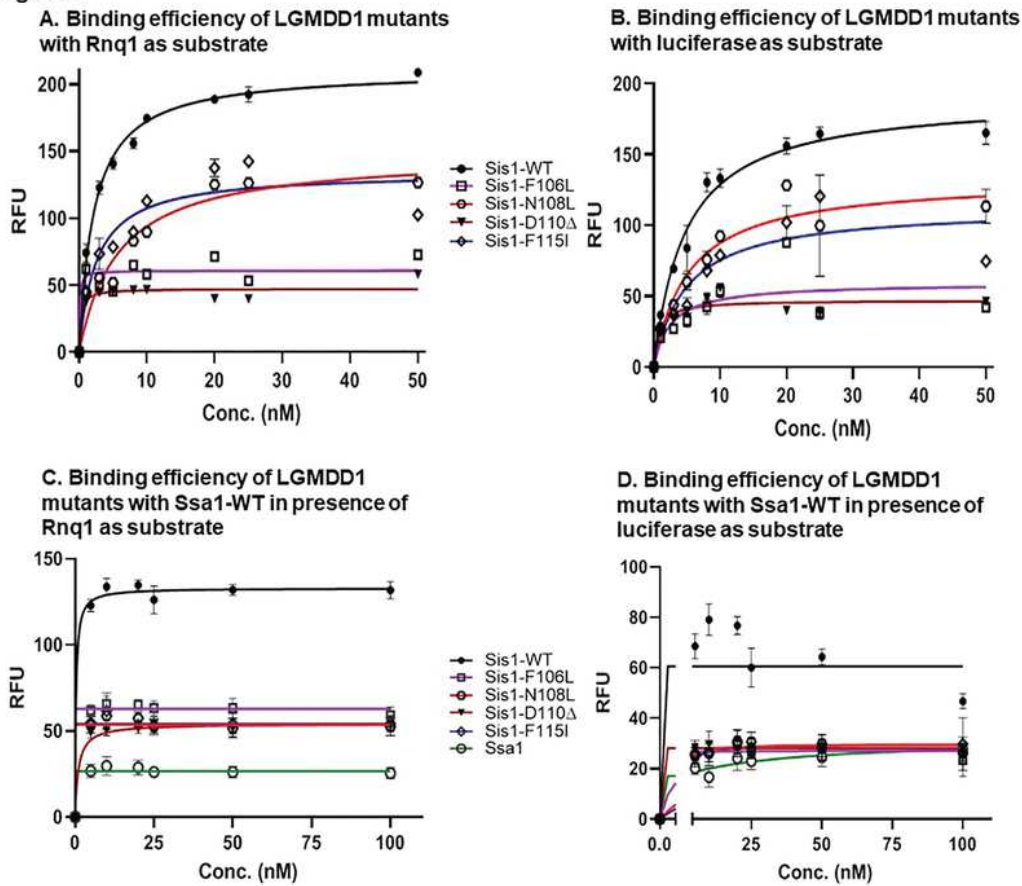


Figure 4. **Sis1 binding to both substrate and Hsp70 is compromised in the presence of LGMDD1 G/F domain mutants.** Binding of purified Sis1-WT (black), Sis1-F106L (purple), Sis1-N108L (red), Sis1-D110Δ (brown), or Sis1-F115I (blue) to denatured Rnq1 (A) and luciferase (B) Rnq1 (400 ng) and luciferase (100 ng) immobilized in microtiter plate wells and dilutions of purified Sis1-WT and Sis1-mutants (0, 1, 3, 5, 8, 10, 20, 25, 50 nM) were incubated with each substrate. The amount of Sis1 retained in the wells after extensive washings was detected using a Sis1 specific antibody. Denatured Rnq1 (C) and denatured luciferase (D) were premixed with Sis1-WT/mutants and immobilized in microtiter plate wells and dilutions of Ssa1-WT (0-100 nM) were incubated with it. Bound Ssa1-WT was detected using an  $\alpha$ Ssa1 antibody. For A-D, Sis1-WT was compared to LGMDD1 mutants. For (A-D), values shown are \*\*\* $p < 0.001$ .

Figure 4

See figure for legend.

Figure 5

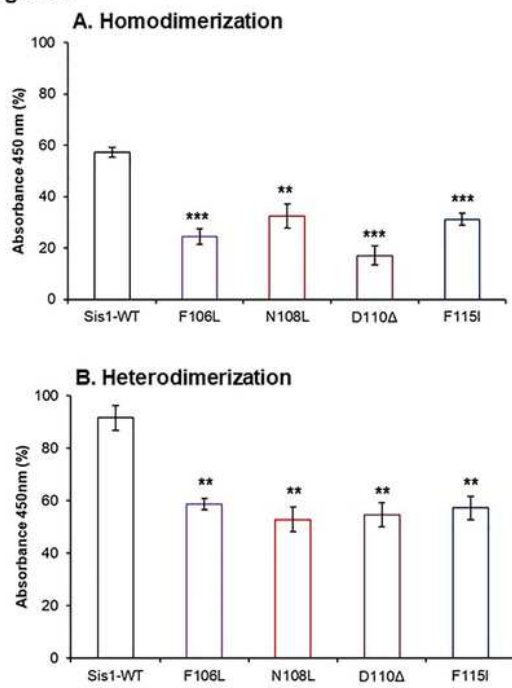


Figure 5. **LGMD1 G/F domain mutants were defective in dimerizing.** (A) For homodimerization, uncleaved His-tagged Sis1-WT and mutants (20 nM) were added into non-His-tagged (cleaved) Sis1-WT and mutants (200 nM) and adsorbed in microtiter plate wells. (B) For heterodimerization, uncleaved His-tagged Sis1-WT (20 nM) was added to cleaved mutants (200 nM) and adsorbed in microtiter plate wells. In both (A) and (B), following adsorption, ELISA was performed using an anti-His antibody. All LGMD1 mutants were compared with Sis1-WT.

Figure 5

See figure for legend.

Figure 6

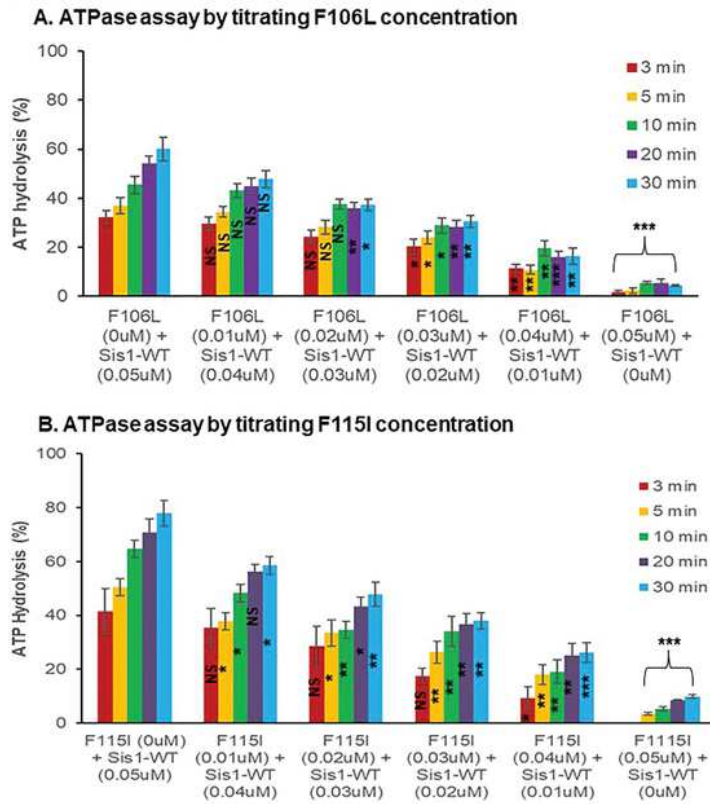


Figure 6. **LGMD1 G/F domain mutants inhibit Sis1-WT induced ATPase activity of Ssa1.** Stimulation of Ssa1 ATPase activity in the presence of Rnq1 seeds formed at 18°C. Sis1-mutants (Sis1-F106L (A), or Sis1-F115I (B)) (0-0.05  $\mu$ M) were titrated with Sis1-WT (0-0.05  $\mu$ M) in the presence of Ssa1 (1  $\mu$ M) and ATP (1 mM). The fraction of ATP converted to ADP was determined at various time-points from 3 to 30 minutes. Values of the increasing concentration of LGMD1 mutants (0.01-0.05  $\mu$ M) were compared with Sis1-WT (0.05  $\mu$ M) alone.

Figure 6

See figure for legend.

Figure 7

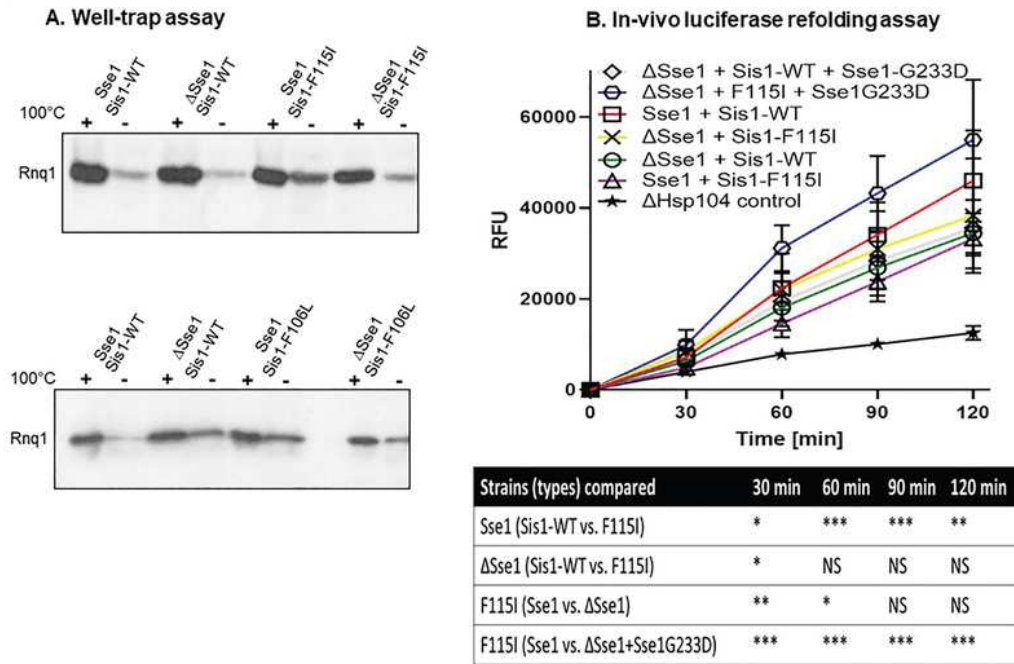


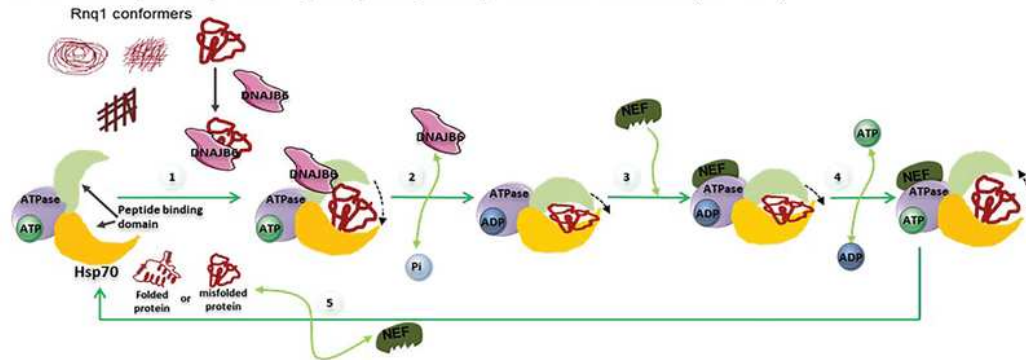
Figure 7. **Deletion or inhibition of Sse1 function rescues prion propagation of [RNQ+] and restored impaired FFL refolding.** (A) Deletion of Sse1 partially suppresses prion loss caused by LGMDD1 mutants. Analysis of prion propagation in Sse1 and  $\Delta$ Sse1 strains harboring s. d. medium [RNQ+], expressing either Sis1-WT or Sis1-F115I or Sis1-F106L by well-trap assay. Cell lysates were incubated at room temperature (-) or 100°C and subjected to SDS-PAGE and western blot using an  $\alpha$ Rnq1 antibody. Rnq1 that is not sequestered in aggregates will enter the gel in the unboiled sample, which indicates destabilization of the [RNQ+] prion. (B) The refolding of firefly luciferase (FFL) was measured in the Sse1 and  $\Delta$ Sse1 yeast cells carrying Sis1-WT, LGMDD1 mutant (Sis1-F115I), and Sse1 mutant (Sse1-G233D) along with a plasmid expressing FFL. Yeast were normalized, treated with cycloheximide, and subjected to heat shock at 42°C for 22 minutes, followed by recovery at 30°C. Luminescence was measured at the indicated time points during recovery. Values shown are  $\pm$  SEM of at least three independent experiments.

Figure 7

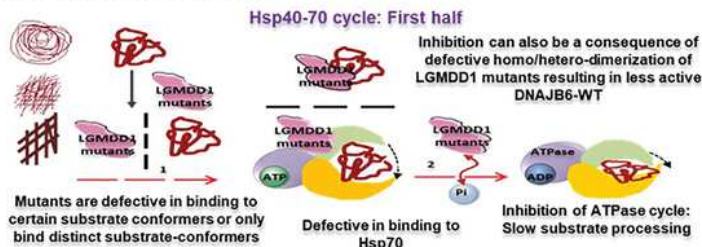
See figure for legend.

Figure 8

A. Normal Hsp40-Hsp70 ATP hydrolysis cycle in presence of DNAJB6 (Sis1-WT)



B. LGMDD1 mutants inhibit Hsp70/40 cycle



C. Possible therapeutic route

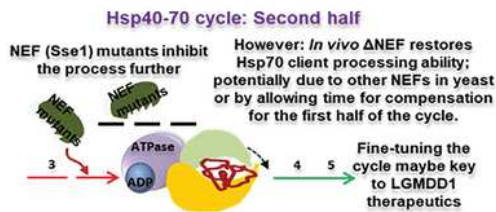


Figure 8. Schematic diagram depicting possible mechanism of LGMDD1 mutants and their effects on the Hsp70 ATPase cycle, as well as proposed therapeutic intervention. (A) Cartoon depicting the normal processing of one of the conformers (substrate) of an aggregated protein, mediated by DNAJB6 (Hsp40) through the Hsp70 ATPase cycle. The **green** arrows throughout the cycle indicate normal functioning. (B) Cartoon depicting possible mechanistic insights as to how LGMDD1 G/F domain mutants delay or inhibit the Hsp70 ATPase cycle. The dashed **red** arrows indicate inhibition. Mutants were inefficient in terms of both homo and hetero-dimerization and that may be related to their reduced ability to assist Hsp70 in protein folding. In the first half of the Hsp70 ATPase cycle, LGMDD1 mutants were incompetent in their ability to bind specific substrate conformers and Hsp70, which delays the downstream processing of the substrate through Hsp70-ATPase cycle. This inhibition could negatively impact Hsp70-mediated ATP-hydrolysis. (C) Possible therapeutic route. In the second half of the cycle, NEF mutants inhibit the binding and exchange of nucleotide, which delay the downstream process of substrate release in the cycle. However, this delay led to positive consequences in terms of yeast prion propagation. Overall, altering the balance between the two halves of the Hsp70-ATPase cycle may provide a key step to consider for therapeutic intervention for these types of diseases.

Figure 8

See figure for legend.

## Supplementary Files

This is a list of supplementary files associated with this preprint. Click to download.

- [SupplementaryFigures.pdf](#)